On the Effect of Flow Direction on Mixed Convection from a Horizontal Cylinder in a Saturated Porous Medium

Mohammed A. Ahmed
Mechanical Engineering Department, University of Anbar

ABSTRACT
A numerical investigation of mixed convection from a horizontal cylinder in a saturated porous medium is presented. The governing equations based on Darcy's law are expressed in a body- fitted coordinate system and solved numerically by explicit method. The direction of the flow varies between the vertically up ward(assisting flow) and vertically downward(opposing flow). Results are presented for Reynolds number Re from 10 to 100 with Grashof numbers up to Gr =5Re. The Prandtl number was kept at a constant value of 0.7. results are presented for the streamlines and isotherms as well as the local and average Nusselt number at different values of governing parameters. Comparison with previous theoretical results show good agreement.

Key words: Mixed convection, Porous medium, Constant surface temperature, Numerical results.

تأثير اتجــاه الجريان على الحمل المختلط من اسطوانة أفقيــة في وســط مسامي مشبع

محمد عبد احمد
قسم الهندسة الميكانيكية، جامعة الانبار

الخلاصة

أجريت دراسة عددية للحمل المختلط من اسطوانة أفقية في وسط مسامي مشبع. المعادلات الحاكمة المعتمدة على قانون دارسي تم التعبير عنها بنظام مطابقة إحداثيات الجسم وحلت عدديا بالطريقة البينية. اتجاه الجريان يتغير بين شاقوليا باتجاه الأعلى إلى شاقوليا باتجاه الأسفل. النتائج مثلت لعدد رينولدز من ١٠ إلى ١٠٠ مع عدد كر شوف إلى (٥ *عدد رينولدز).مع بقاء قيمة عدد براندتل ثابتة عند القيمة ٠.٧ . مثلت النتائج لخطوط الانسياب ، درجة الحرارة و عدد نسلت الموضعي والمعدل عند قيم مختلفة للمتغيرات الحاكمة. المقارنة مع نتائج نظرية سابقة توضح توافق جيد.

1. INTRODUCTION

Heat transfer from a circular cylinder buried in a saturated porous medium has a great practical importance in many engineering applications. These applications include the utilization of geothermal energy, the control of pollutant spread in ground water, nuclear engineering, compact heat exchangers, solar power collectors and high- performance insulation for buildings. The problem of mixed convection over a horizontal, isothermal cylinder embedded in a saturated porous medium was studied by Cheng(1982) using boundary layer approximation. Later, the problem was extended to include a non isothermal cylinder by Minkowy etal.(1985) and constant flux cylinder by Huang etal.(1986). All three above studies treated the case of assisting flow only. Numerical results based on series solutions were obtained by Badr and Pop(1988)for assisting and opposing flows over a horizontal cylinder. Zhou and Lai(2002) considered the same problem were solved by Badr and Pop(1988) based on Darcy's law and using finite difference method with body-fitted coordinates. Experimental results were very few and were reported only by Fand etal. (1987) for cross flow over a horizontal cylinder.

However, the purpose of the present work is to study the effect of flow direction on mixed convection from isothermal cylinder embedded in a saturated porous medium. Since there is no prior study was done for study the effect of flow direction on mixed convection from cylinder.

2. MATHMATICAL FORMULATIONS

2.1 Governing Equations

The present paper studied the problem of mixed convection around isothermal cylinder embedded in a porous medium(Fig. 1). Since the cylinder is maintained at constant temperature T_w which is assumed sufficiently higher than the ambient fluid temperature $T\infty$ ($T_w > T\infty$), thermal buoyancy is present in the flow field. To approximate the mixed heat convection flow problem, several assumptions have been made. The flow is steady, in compressible and two dimension. The properties of the porous medium and the fluid are isotropic and homogeneous. With these assumptions, the governing equations based on the Darcy's law are given by (Zhou and Lai, 2002)

$$\frac{\partial u}{\partial x}+\frac{\partial v}{\partial y}=0 \tag{1}$$

$$u=\frac{-k}{\mu}\left(\frac{\partial p}{\partial x}+\rho.g\beta\cos\lambda\right) \tag{2}$$

$$v=\frac{-k}{\mu}\left(\frac{\partial p}{\partial y}+\rho.g\beta\sin\lambda\right) \tag{3}$$

$$\sigma\frac{\partial T}{\partial t}+u\frac{\partial T}{\partial x}+v\frac{\partial T}{\partial y}=\alpha\left(\frac{\partial^2 T}{\partial x^2}+\frac{\partial^2 T}{\partial y^2}\right) \tag{4}$$

the stream function ψ is related to the velocity components by

$$u=\frac{\partial\psi}{\partial y}\qquad v=-\frac{\partial\psi}{\partial x} \tag{5}$$

The above governing equations can be simplified to give.

$$\frac{\partial^2\psi}{\partial x^2}+\frac{\partial^2\psi}{\partial y^2}-\frac{kg\beta}{\nu}\left(\frac{\partial T}{\partial x}\sin\lambda-\frac{\partial T}{\partial y}\cos\lambda\right)=0 \tag{6}$$

$$\sigma\frac{\partial T}{\partial t}+\frac{\partial\psi}{\partial y}\frac{\partial T}{\partial x}-\frac{\partial\psi}{\partial x}\frac{\partial T}{\partial y}=\alpha\left(\frac{\partial^2 T}{\partial x^2}+\frac{\partial^2 T}{\partial y^2}\right) \tag{7}$$

Further, the above governing equations can be transformed to dimensionless form as shown below.

$$\frac{\partial^2\Psi}{\partial X^2}+\frac{\partial^2\Psi}{\partial Y^2}+\frac{Gr}{\mathrm{Re}}\left(\frac{\partial\theta}{\partial X}\sin\lambda-\frac{\partial\theta}{\partial Y}\cos\lambda\right)=0 \tag{8}$$

$$\frac{\partial\theta}{\partial\tau}+\frac{\partial\Psi}{\partial Y}\frac{\partial\theta}{\partial X}-\frac{\partial\Psi}{\partial X}\frac{\partial\theta}{\partial Y}=\frac{1}{\mathrm{Re}.\mathrm{Pr}}\left(\frac{\partial^2\theta}{\partial X^2}+\frac{\partial^2\theta}{\partial Y^2}\right) \tag{9}$$

The corresponding boundary conditions used for computations are given as follows:

At inlet flow $\theta = 0, \quad \Psi = Y$ (10a)

On the cylinder wall $\Psi = 0, \theta = 1$ (10b)

At upper boundary $\Psi = 1, \quad \frac{\partial\theta}{\partial Y}$ (10c)

At lower boundary $\Psi = -1, \quad \frac{\partial\theta}{\partial Y}$

(10d)

At the downstream $\frac{\partial\Psi}{\partial X}=0, \frac{\partial\theta}{\partial X}=0$ (10e)

In terms of the body-fitted coordinates, the governing equations are given by

$$\frac{1}{J}\left[\lambda'.\frac{\partial\Psi}{\partial\zeta}+\sigma'.\frac{\partial\Psi}{\partial\eta}+\alpha'.\frac{\partial^2\Psi}{\partial\zeta^2}-2\beta'.\frac{\partial^2\Psi}{\partial\zeta\partial\eta}+\gamma'.\frac{\partial^2\Psi}{\partial\eta^2}\right]+\frac{Gr}{\mathrm{Re}}\left[\left(\frac{\partial\theta}{\partial\zeta}.\frac{\partial Y}{\partial\eta}+\frac{\partial\theta}{\partial\eta}.\frac{\partial Y}{\partial\zeta}\right)\sin\lambda\right.$$
$$\left.-\left(\frac{\partial\theta}{\partial\eta}.\frac{\partial X}{\partial\eta}-\frac{\partial\theta}{\partial\zeta}.\frac{\partial X}{\partial\eta}\right)\cos\lambda\right]=0 \tag{11}$$

$$\frac{\partial\theta}{\partial\tau}+\frac{1}{J}\left[-\frac{\partial\Psi}{\partial\zeta}.\frac{\partial\theta}{\partial\eta}+\frac{\partial\Psi}{\partial\eta}.\frac{\partial\theta}{\partial\zeta}\right]=\frac{1}{\mathrm{Re}.pr.J^2}\left[\lambda'.\frac{\partial\theta}{\partial\zeta}+\sigma'.\frac{\partial\theta}{\partial\eta}+\alpha'.\frac{\partial^2\theta}{\partial\zeta^2}-2\beta'.\frac{\partial^2\theta}{\partial\zeta\partial\eta}+\gamma'.\frac{\partial^2\theta}{\partial\eta^2}\right] \tag{12}$$

In the discretization of the equations, the time dependent term is approximated by forward difference, the diffusion and convection terms by central difference. Theoretically the accuracy of solutions is of the first order. Since a small grid size and time step have been used, it is expected that the solutions are reasonably accurate. The computational domain covers a region that extends 5d in x-direction and 3d in y- direction. A uniform grid, 99x40, in

the transformed computational domain was considered suitable for covering the computational domain. The dimensionless time step used in the present study was 10^{-4}.

2.2 Calculation of Nusselt Number

When the solution convergence criterion is reached, the local and mean Nusselt numbers on the cylinder walls are calculated. From the balance of heat flux at the surface, the Nusselt number can be obtained as

$$Nu = -\frac{\partial \theta}{\partial n} \tag{13}$$

Now, Equation(13) is transformed into general coordinate(ζ,η) as follows (Broughton etal., 1986)

$$Nu = \frac{1}{J\sqrt{\gamma'}}\left[\gamma'.\theta_{\eta} - \beta'.\theta_{\xi}\right] \tag{14}$$

Since the temperature along the wall cylinder(w)is constant, $\theta_{\xi} = 0$, Equation(14) becomes:

$$Nu = \frac{\gamma'}{J\sqrt{\gamma'}}\theta_{\eta} \tag{15}$$

The Nusselt number in Equation (15) is the local Nusselt number. To find the average Nusselt, the local Nusselt number should be integrated by using numerical integration (Al-Khafaji etal.,1986).

3. RESULTS AND DISCUSION

In the present work, detailed parametric studies are conducted using a two-dimensional model based on the assumption that the cylinder is long enough for axial effects to be neglected. Figure 2 shows the flow and temperature fields at Re =20, Gr =20 and different values of of λ. It is found that the effect of thermal buoyancy on the flow and temperature fields depends on the forced flow direction. At low value of Grashof numbers(Gr =20), the flow field is perturbed by thermal buoyancy. With an increase in the Grashof number(Fig. 3), more fluid is accelerated through the central region for $\lambda=0^{o}$. As a result, the thermal plume is extended downstream.

On the other hand, When $\lambda=180^{o}$ a buoyancy-induced recalculating cell is present near the cylinder and thermal plume extended both upstream and downstream. It can also be seen from these figures, the flow and temperature fields are symmetrical about x-axis, when the forced flow direction is vertically upward or vertically downward. Otherwise, the fields become asymmetric.

Figure 4 gives the local Nusselt number distribution around the cylinder at Re =20 and different values of Gr and λ. It is found that the local Nusselt number distribution is greatly affected by the direction of the forced flow. At low value of Grashof number(Fig. 4(a)), the maximum and minimum Nusselt numbers occur at stagnation and rare stagnation points respectively for all directions of forced flow.

As Grashof number increase (Fig. 4(b)), the maximum and minimum Nusselt numbers continue to occur at stagnation and rare stagnation points respectively for assisting flow. In opposing flow, the local Nusselt number decrease at stagnation point and increase at rear

stagnation point. This is expected to occur as a strength of rotating cell increase with increase of Grashof number.

Figure 5 shows the average Nusselt number at various directions. It is found that the average Nusselt number decrease as λ increases. As Grashof number increase, the average Nusselt number increase for $\lambda < 135^o$ and decrease when $\lambda \geq 135^o$.

Figure 6 shows that the mean Nusselt number obtained in the present study are in good agreement with those obtained by previous work.

Figure 7 depicts the present results of flow and temperature fields show good agreement with numerical study by Zhou and Lai.

4. CONCLUSIONS

A numerical simulation has been performed for the problem of the mixed convection from a cylinder embedded in a saturated porous medium. The results for mean Nusselt number show good agreement with other published results. The paper gives detailed analysis of the local and the average Nusselt number with different Reynolds numbers, Grashof number and the forced flow directions. The following conclusion can be drawn from the paper.

1. Forced flow direction has a strong effect on the distributions of Nusselt number. The values of local Nusselt number decrease over most of the cylinder surfaces as (λ) increases.
2. At low value of Grashof number, the average Nusselt number decreases as(λ) increases. As Grashof number increases, the average Nusselt number increases monotonically for ($\lambda \leq 135^o$), while, the average Nusselt number decreases for ($\lambda > 135^o$) as Grashof number increases.

REFERENCES

[1] AL-Khafaji, A., W. & Tooley, J., R., *Numerical Methods in Engineering Practice*, 1st Edition, CBS Publishing, Japan Ltd, 1986.

[20 Broughton, R., C. & Oliver, A., J., *A Numerical Model for Convection in Complex–Dimensional Geometries and it is Application to Buoyancy flow in Power Cable*, International Heat Transfer Conferences, vol. 2, pp. 447 - 451, 1986.

[3] Badr, H. M., and Pop, I., *Combined Convection from an Isothermal Horizontal Rod Buried in a Porous Medium,* Int. J. Heat and Mass Transfer, vol. 31, no. 12, pp. 2527 - 2541, 1988.

[4] Cheng, P., *Mixed Convection about a Horizontal Cylinder and Sphere in a fluid-Saturated Porous Medium,* Int. J. Heat and Mass Transfer, vol. 25, no. 8, pp. 1245 - 1247, 1982.

[5] Fand, R. M., and Phan, R. T., *Combined Forced and Natural Convection Heat Transfer from a Horizontal Cylinder Embedded in a Porous Medium,* Int. J. Heat and Mass Transfer, vol. 30, no. 7, pp. 1351 - 1358, 1987.

[6] Huang, M. J., Yih, K. A., Chou, Y. L., and Chen, C. k., *Mixed Convection Flow over a Horizontal Cylinder or Sphere Embedded in a Saturated Porous Medium,* J. Heat Transfer, vol. 108, no. 2, pp.469 - 471, 1986.

[7] Minkowycz, M. J., Cheng, P., and Chang, C. H., *Mixed Convection about a non Isothermal Cylinder and Sphere in a Porous Medium, Numerical* Heat Transfer, vol. 8, no.3, pp.349 - 359, 1985.

[8] Zhou, M. J., and Lai, F.C, *Aiding and Opposing Mixed Convection from a Cylinder in a Saturated Porous Medium,* J. Porous Media, vol. 5, no. 2, pp.103 - 111, 2002.

NOMENCLATURE

List of symbols

d	cylinder diameter,(m)
g	gravity acceleration,(m/s^2)
Gr	Grashof number, $kg\beta(T_w- T_\infty).d /\upsilon^2$
n	outer normal vector
Nu	local Nusselt number (h.d/k)
$\overline{Nu}$	average Nusselt number ($\overline{h}$.d/k)
h , $\overline{h}$	local and average heat transfer coefficients, ($w/m^2.k$)
J	Jacobain of transformation
K	porous medium permeability,(m^2)
k	thermal conductivity of porous medium, (w/m.k)
p	pressure,(pa)
Pr	Prandtl number, (υ/ α)
Re	Reynolds number, (u_∞.d/ υ)
t	time, (s)
T	temperature, (k)
u ,v	Darcy velocities components,(m/s)
u_∞	free stream velocity,(m/s)
x, y	cartesian coordinates,(m)
X, Y	dimensionless Cartesian coordinates, (X=x/d , Y=y/d)

Greek symbols

ζ , η	body-fitted coordinates
α	thermal diffusivity of porous medium, $k_m/(\rho\, cp)_f$ (m^2/s)
α', β', λ', γ'	transforming coefficients
β	thermal expansion coefficient, (k^{-1})
ρ	density of fluid, (kg/m^3)
υ	kinematic viscosity, (m/s^2)
σ	ratio of thermal capacities between porous medium and fluid, $(\rho cp)_m / (\rho\, cp)_f$
τ	dimensionless time, ($t\, u_\infty/\sigma.d$)
λ	free stream direction
γ	angular position
ψ	stream function
Ψ	dimensionless stream function, ($\psi/d.u_\infty$)
θ	dimensionless temperature, $(T - T_\infty) /(T_w – T_\infty)$

Subscripts

f	fluid
m	porous medium
w	wall
∞	free stream

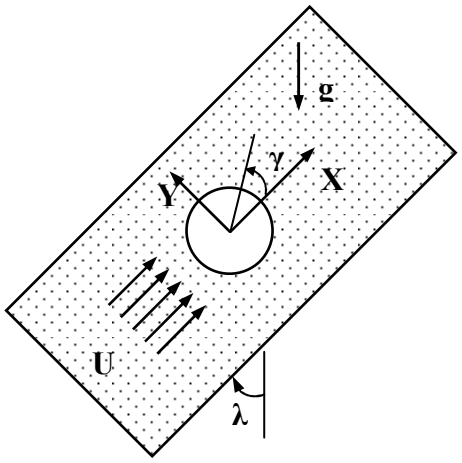

Fig. 1. Mixed convection from a horizontal cylinder embedded in a porous medium.

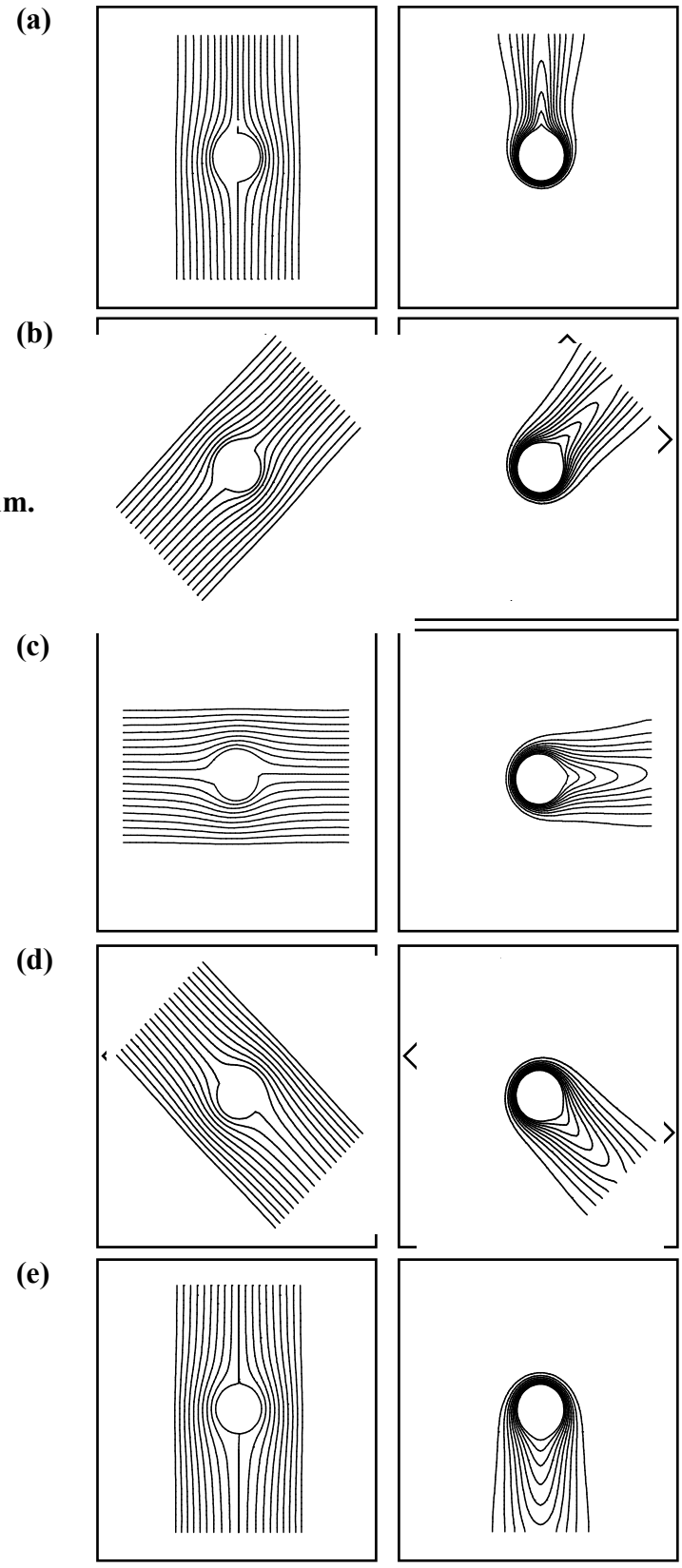

Fig. 2. Streamline (left) and isotherms (right) contours at Re=20 and Gr=20: (a) $\lambda=0^o$, (b) $\lambda=45^o$, (c) $\lambda=90^o$, (d) $\lambda=135^o$, (e) $\lambda=180^o$

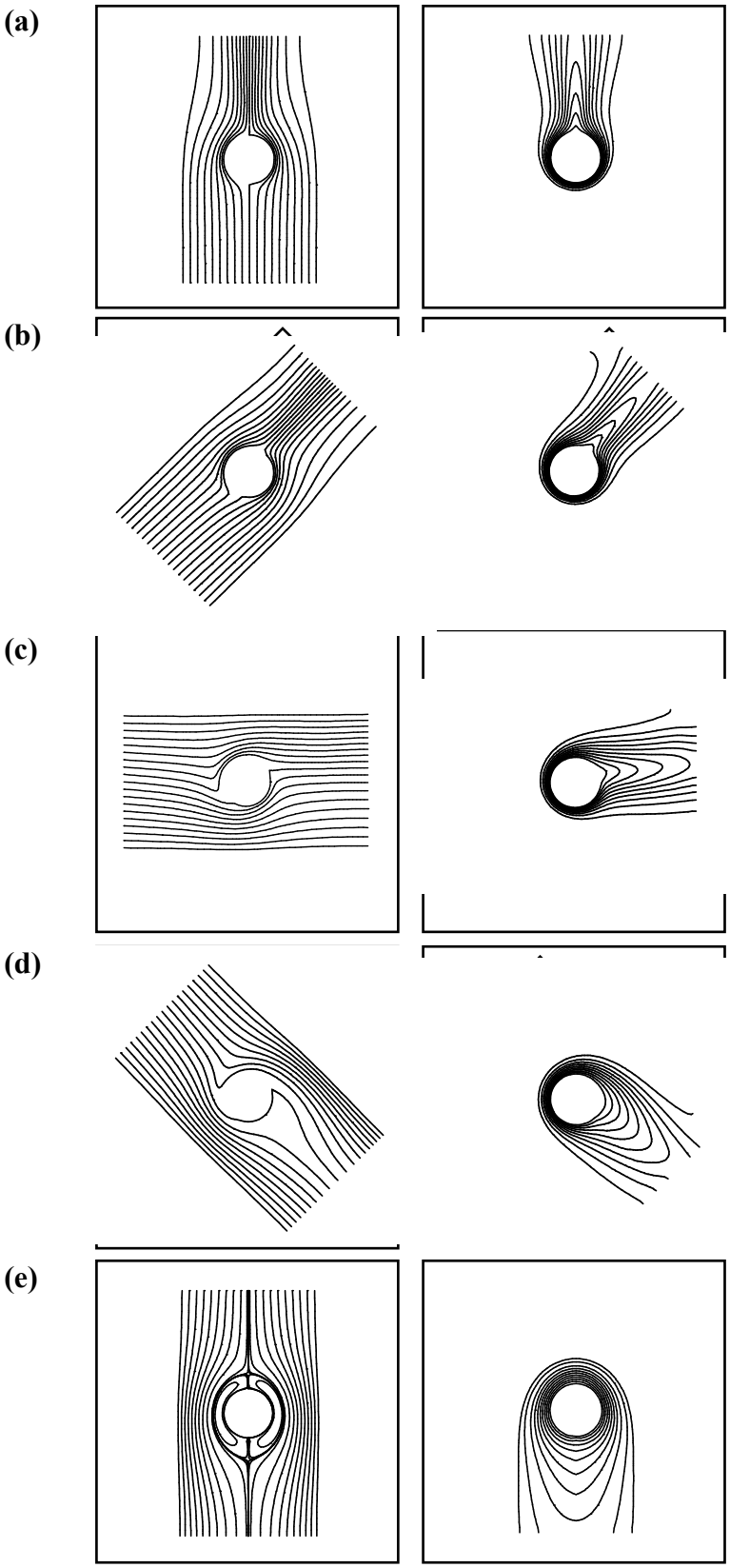

Fig. 3. Streamline (left) and isotherms(right) contours at Re=20 and Gr=100: (a) $\lambda=0^o$, (b) $\lambda=45^o$, (c) $\lambda=90^o$, (d) $\lambda=135^o$, (e) $\lambda=180^o$

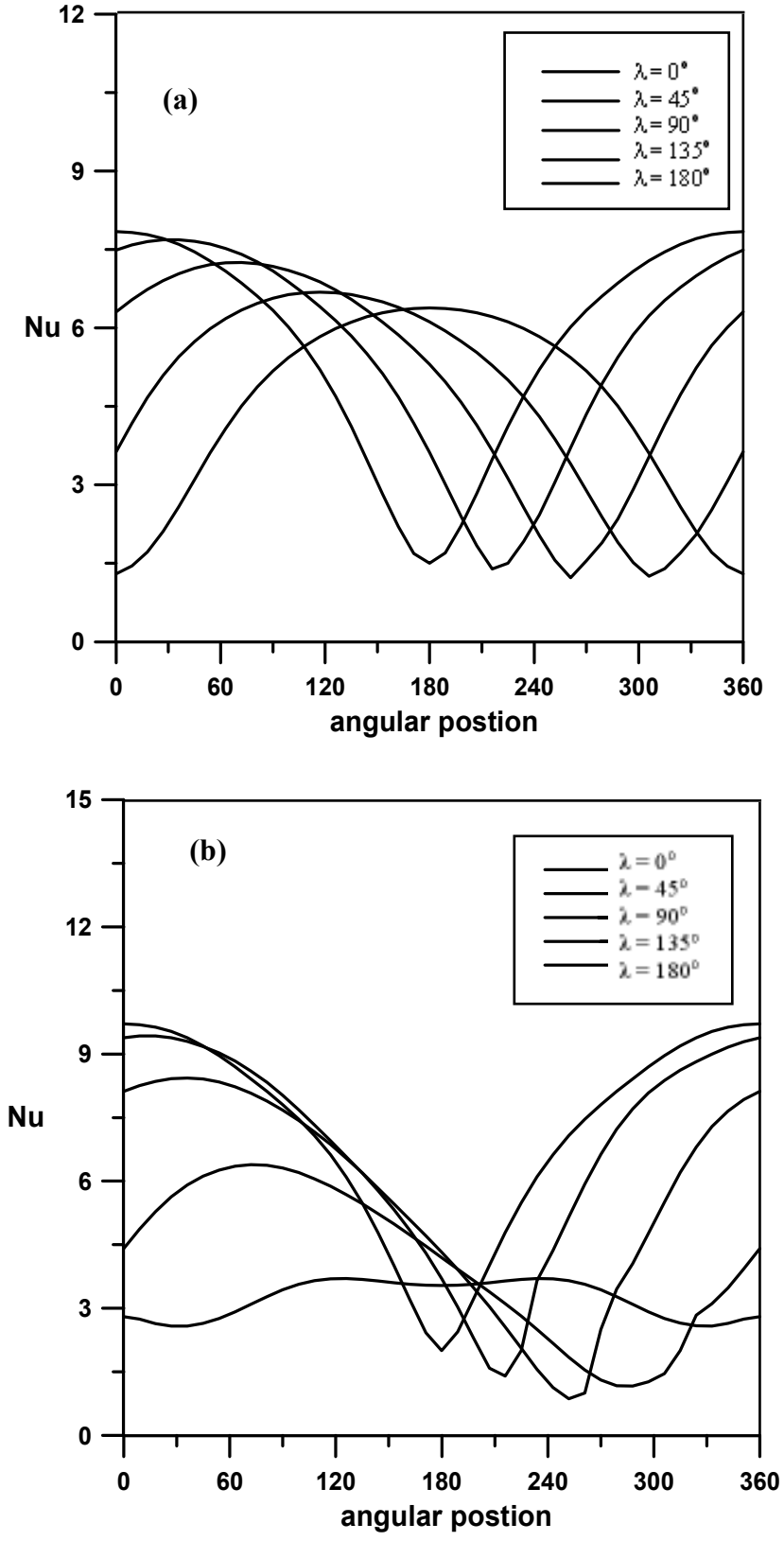

Fig. 4. Effect of forced flow direction on the Local Nusselt number distribution for case of Re =20: (a)Gr = 20, (b) Gr =80.

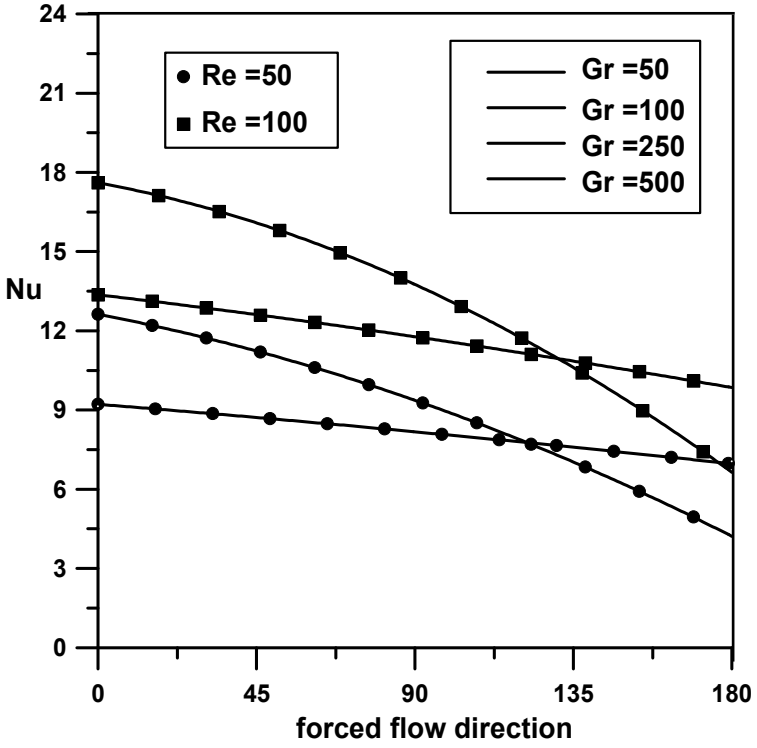

Fig. 5. Effect of forced flow direction on the average Nusselt number for Re =50, Re =100 and different values of Gr.

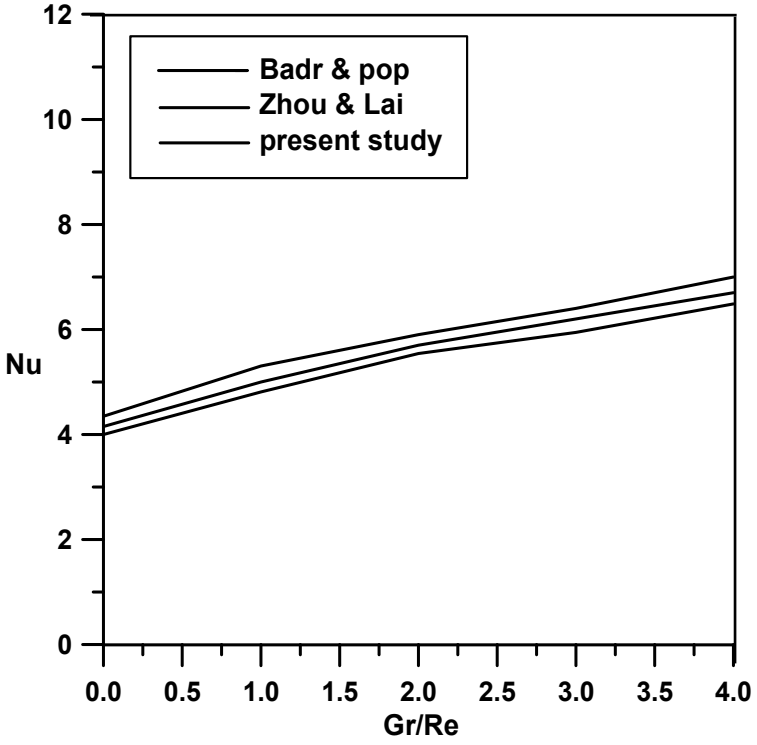

Fig. 6. Comparison between present work and previous theoretical results at Re =20 and $\lambda = 0^{o}$.

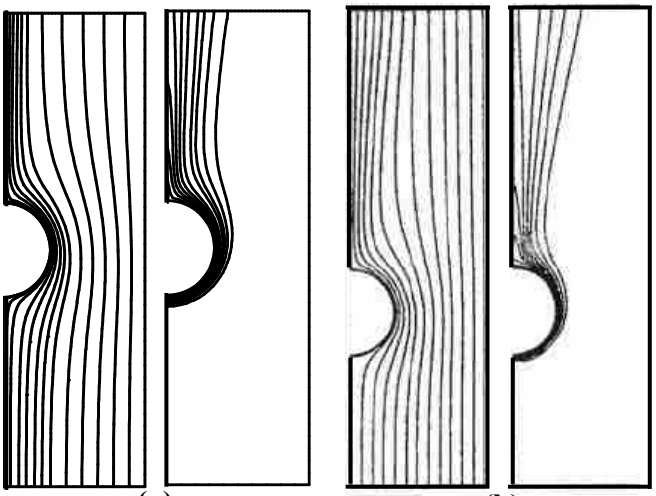

Fig. 7. Comparison of temperature and flow fields for assisting flow at Re =100 and Gr = 400: (a)present study, (b)previous study Zohu and Lai .